ADVANCED FUNCTIONAL MATERIALS
www.afm-journal.de

Materials Views
www.MaterialsViews.com

Level Set Photonic Quasicrystals with Phase Parameters

*Lin Jia, Ion Bita, and Edwin L. Thomas**

A systematic study of the photonic band gap (PBG) properties of 8-, 10- and 12-fold rotational symmetric quasicrystals (QCs) defined by level set equations with various phase parameters is reported. The optimized filling ratios corresponding to the largest PBGs for 19 types of QCs are found, which are useful for photonic QC fabrication design. The impact of filling ratio, rotational symmetry, and experimental fabrication parameters on the resultant PBGs are studied via PBG maps calculated by finite-difference time-domain (FDTD). Large area, high quality 8-, 10-, and 12-fold quasicrystalline pattern fabrication using multiple exposure interference lithography (MEIL) is also demonstrated.

1. Introduction

Quasicrystals (QCs) are interesting aperiodic crystals with rotational symmetries forbidden in conventional periodic crystals. QCs break translational periodicity while maintaining a well-defined and long-range ordered structure, as evident from their diffraction spectra consisting of sharp peaks.[1] Two-dimensional (2D) photonic QCs, first proposed in 1998,[2] have higher rotational symmetries than photonic crystals and demonstrate interesting optical properties including isotropic photonic band structures,[3,4] defect-free localized modes,[5–7] multiple band gaps,[8,9] and the possibility to open a photonic band gap (PBG) at quite low refractive index contrast.[10,11] Therefore photonic QCs are excellent candidates for various photonic applications, including lensing,[12] waveguiding,[13–16] negative refraction,[17] nonlinear interaction,[8,18] optical fiber devices,[19] plasmonics,[20] photonic gels[21,22] and energy applications.[23,24] An important subgroup of QCs are those defined by level set equations, since these can be fabricated by multiple exposure interference lithography (MEIL).[25–30]

In this letter, we systematically study the PBG properties of 8-, 10- and 12-fold rotational symmetric QCs defined by level set equations with nine different phase parameters. Compared to previous studies,[9,31] the current work is more comprehensive: various phase parameters and a wide filling ratio range (0.02 to 0.98) are investigated. The local density of states (LDOS) plots for corresponding QCs are assembled to 19 PBG maps to indicate the influence of filling ratio, symmetry, and experimental parameters on the associated PBGs. The optimum filling ratios for QCs of 19 types (nine phases and three rotational symmetries) for large PBGs are found. We also demonstrate large area, high quality QC pattern fabrication via MEIL and reactive ion etching (RIE).

2. Theoretical and Experimental Results

The numerical representation of PQC structures is achieved by starting with a model for the 2D spatial distribution of light intensity $I(x, y)$ which is obtained during multiple exposures of one dimensional (1D) fringe patterns from 2-beam interference, with a fixed sample rotation after each exposure. The intensity pattern obtained from interference of two beams is a one dimensional (1D) periodic fringe pattern:

$$I(x, y) = 2I_0\left[1 + \cos(k_x x + k_y y)\right] \quad (1)$$

In Equation (1), I_0 is the light intensity of the beam and $\vec{k} = (k_x, k_y)$ indicates the fringe pattern orientation. Here we assume $I_0 = 1$. The light intensity distribution for N exposures with a fixed rotation between each exposure is:

$$I(x, y) = 2N + \sum_{i=0}^{N-1} 2\cos\left[2\pi x\cos(\pi i/N)/a + 2\pi y\sin(\pi i/N)/a + \varphi\right] \quad (2)$$

The rotational symmetry of the associated QC after N exposures is $2N$. Since high rotational symmetries involve increasing fabrication difficulties due to a reduced structural contrast associated with large number of exposures, we focused our studies on QCs with $N < 7$. For $N = 1, 2, 3$, the structures are periodic. For $N = 4, 5, 6$, the structures are quasiperiodic with 8-, 10-, and 12-fold rotational symmetries respectively. In Equation (2) a is a characteristic unit length and φ is the phase parameter ($0 \le \varphi \le \pi$). The phase parameter φ indicates the relative position between sample rotational center and the fringe pattern. For example, $\varphi = 0$ indicates the rotation center

L. Jia
Institute for Soldier Nanotechnologies
Department of Materials Science and Engineering
Massachusetts Institute of Technology
Cambridge, Massachusetts 02139 USA
Prof. E. L. Thomas
Dean of Engineering
Rice University
P.O. Box 1892, Houston, Texas 77251 USA
E-mail: elt@rice.edu
Dr. I. Bita
Qualcomm MEMS Technologies
San Jose, California 95134 USA

DOI: 10.1002/adfm.201101804

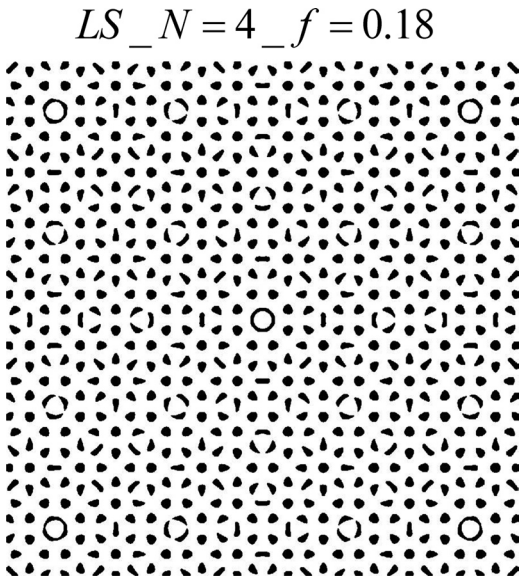

Figure 1. 8-fold rotational symmetric QC. *L S* indicates that the structure is generated from level set Equation (2). The rotational symmetry of the structure is 2*N*. f denotes the filling ratio of the structure. The filling ratio is selected for the largest TM PBG. The phase parameter φ is not involved here because the morphology of the 8-fold rotational symmetric QC is not impacted by the phase parameter.

is at the highest light intensity position of the fringe pattern and $\varphi = \pi$ indicates the rotation center is at the lowest light intensity position. The morphology of 8-fold rotational symmetric QC is not impacted by the phase parameter. Nine representative phase values between 0 and π (i.e. 0 π, 0.125 π, 0.25 π, 0.375 π, 0.5 π, 0.625 π, 0.75 π, 0.875, 1 π) are examined for ten-fold and twelve-fold rotational symmetric QCs. For negative photoresist, the dielectric material occupies all locations where $I(x, y) > I_{cut}$ while air fills the rest of the space. Here I_{cut} corresponds to the photoresist development threshold. By varying the exposure dose, we can numerically represent structures with different fill ratios. Some representative QCs are shown in **Figure 1** (8-fold rotational symmetric QC), **Figure 2** (10-fold rotational symmetric QCs) and **Figure 3** (12-fold rotational symmetric QCs).

For positive photoresist in MEIL, if $f(x, y) < t$, position (x, y) is occupied by material; if $f(x, y) > t$, position (x, y) is occupied by air. The structure with phase parameter φ from the above definition is the same as the structure with phase parameter $\pi - \varphi$ from the definition of negative photoresist, so we only need to discuss negative photoresist.

The absence of translational periodicity in photonic quasicrystals makes the theoretical prediction of their optical properties much more difficult than in the case of photonic crystals. The finite-difference time-domain (FDTD)[32–34] approach to solve Maxwell's equations is particularly well suited for

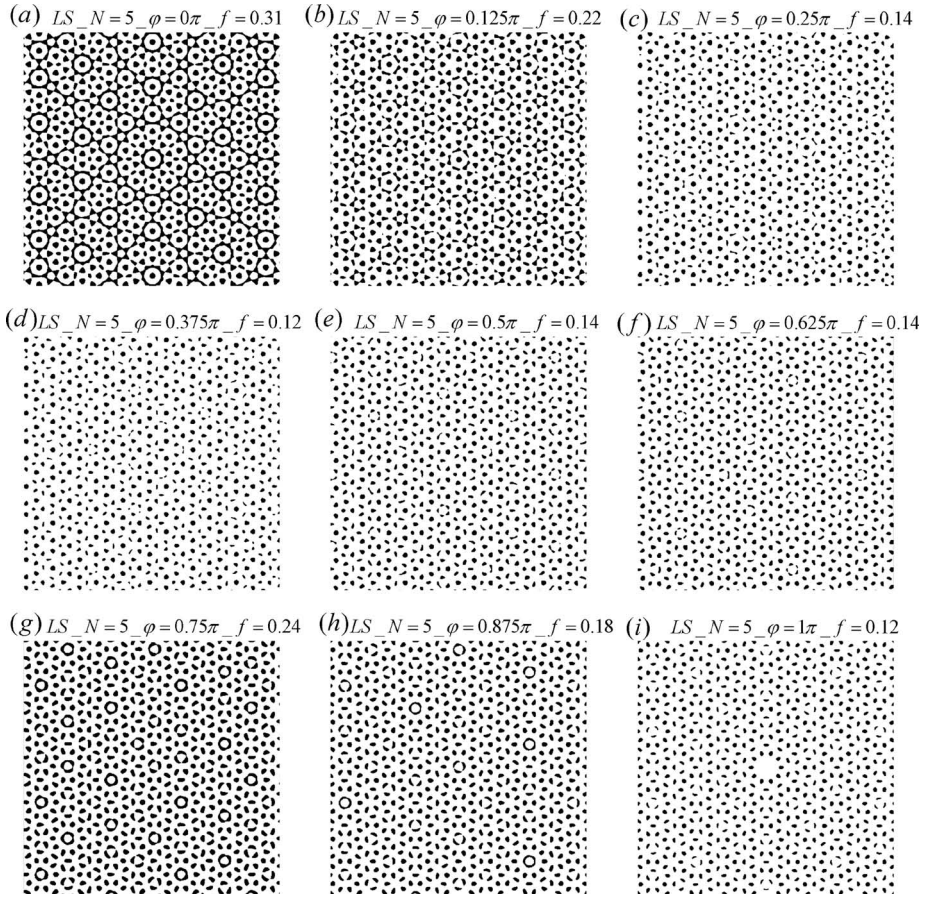

Figure 2. Various 10-fold rotational symmetric QCs. φ is the phase parameter in Equation (2). f denotes the optimized filling ratio for the largest TM PBG.

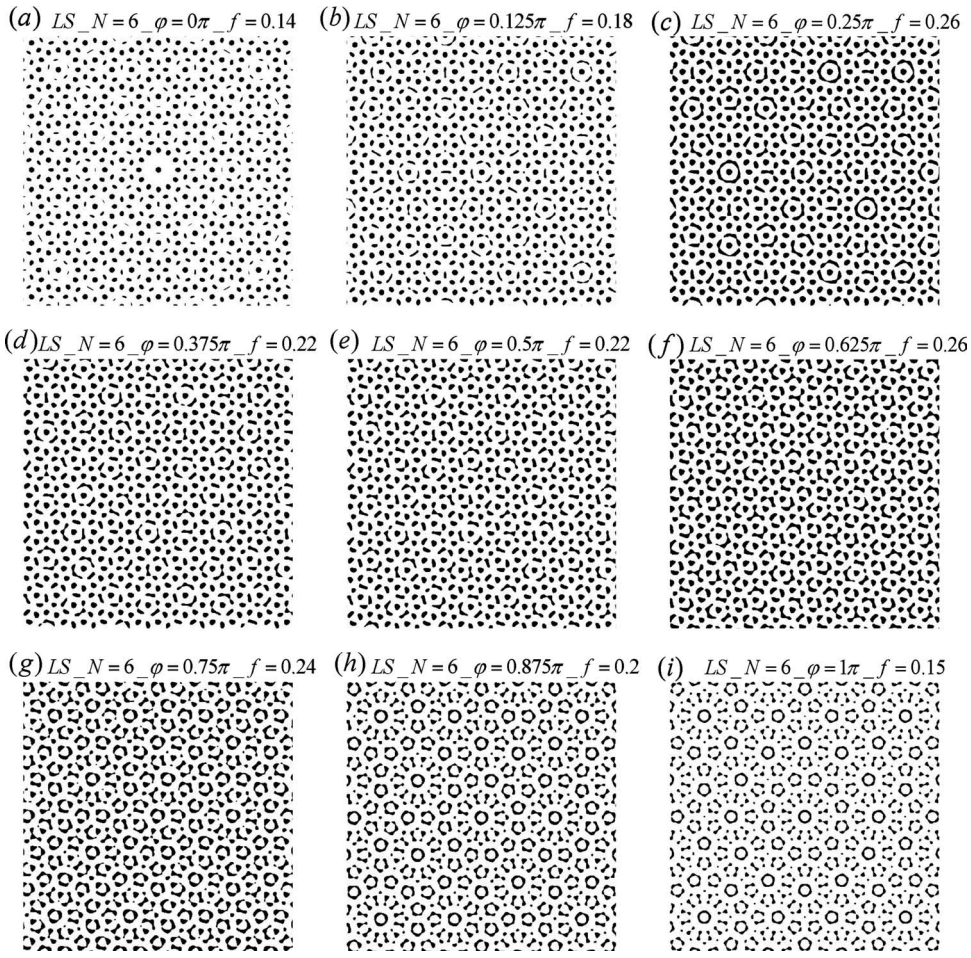

Figure 3. Various 12-fold rotational symmetric QCs.

investigating PBG formation in quasicrystals,[10,35] because it allows the modeling of the optical properties of materials with arbitrary size, shape, and composition. The PBGs of the structures in Figure 1, 2 and 3 were thus determined from the local density of states (LDOS) maps[36–38] computed via FDTD.[34,39]

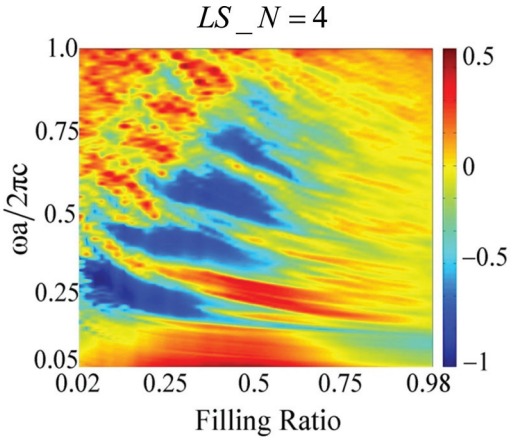

Figure 4. PBG map for 8-fold rotational symmetric QCs.

Here we assume the constitutive materials are silicon and air ($\varepsilon_2 : \varepsilon_1 = 13 : 1$). The transverse electric (TE) PBGs of the QCs in Figure 1 through 3 are trivial; therefore we focus on transverse magnetic (TM) PBGs in this work. The TM PBG maps for 8-, 10- and 12-fold QCs are shown in **Figure 4**, **5**, and **6**. In a PBG map, a continuous low LDOS region along the vertical frequency axis indicates a PBG. According to such maps, the PBGs at different filling ratios can be easily interpreted. Further, multiple gaps are shown, which offer the possibility for nonlinear interactions in a photonic cavity.[8] The largest TM PBGs observed and the associated optimized filling ratios for each type of QCs are shown in **Table 1**.

We fabricated 2D photonic QCs with 8-, l0-, and 12-fold rotational symmetries using MEIL.[27–30] What distinguishes our results from those reported earlier,[40,41] is a ultra-large sample size (up to 2 cm^2), better pattern quality, a reduction in the feature size to 100 nm, along with higher rotational symmetry. The accurate fabrication of QCs at this small length scale, is enabled by the use of an ultra stable Lloyd's mirror interferometer, a short wavelength laser (325 nm HeCd UV laser), and an optically absorbing anti-reflection coating (ARC)[42] underneath the photoresist for accurately recording the low contrast interference pattern. Typical total exposure time is 10 min. The stability of the long exposure comes from high laser quality,

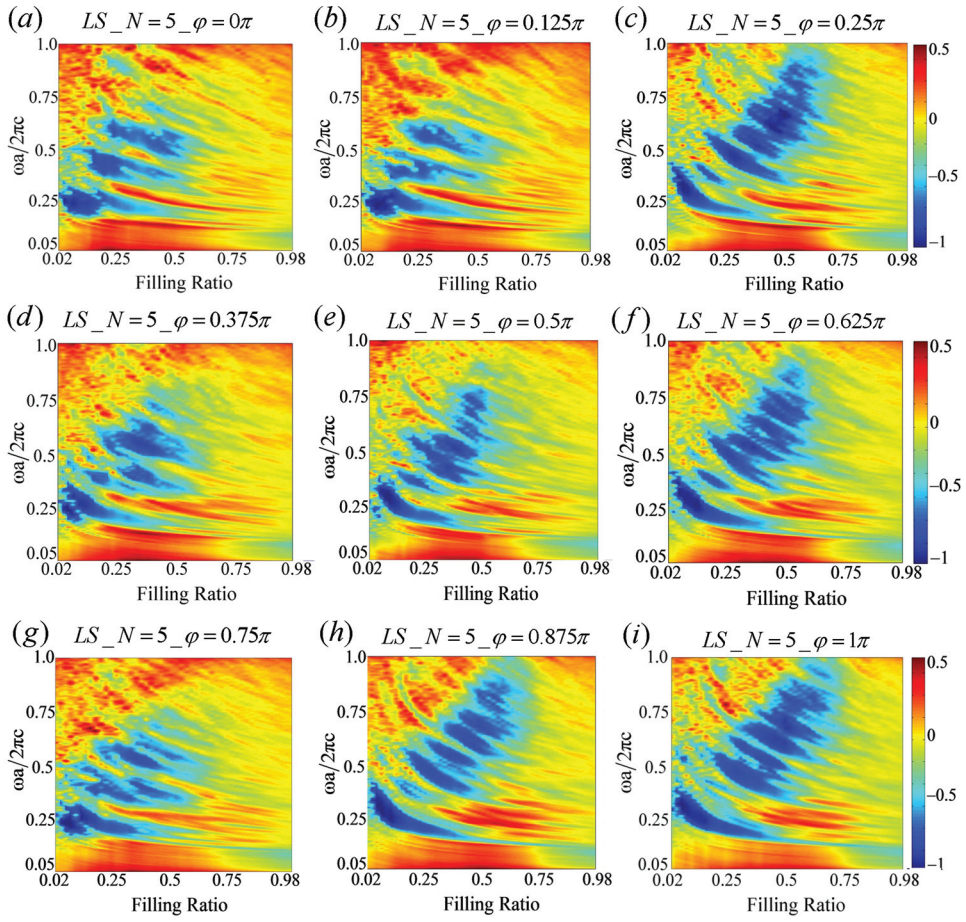

Figure 5. PBG maps for 10-fold rotational symmetric QCs.

the Lloyd's mirror geometry, and the vibration isolation table. The detailed process is shown in **Figure 7**. The diagram of the Lloyd's mirror interferometer is shown in Figure 7a. The laser beam passes through a spatial filter, and expands over a distance of 2 meters, then reaches the sample holder. One dimentional interference pattern is obtained between the reflected portion of the expanded beam and a portion of the beam that is incident directly on the sample substrate holder. The sample stage assembly, which is shown in Figure 7b, is placed on a high accuracy rotation stage. By rotating the stage, and thus changing the incidence angle (θ), as shown in Figure 7c, the spatial period of the interference pattern (P) can be readily changed:

$$P = \lambda / 2\sin(\theta) \tag{3}$$

The sample structure is shown in Figure 7d. The two layers between the 1.5 μm SiO_2 layer and the photoresist are ARC[42] and a 20 nm pattern transfer interlayer. The function of ARC is to minimize the reflection at the bottom interface of the photoresist layer. The pattern transfer interlayer placed between the photoresist and ARC improves the fidelity with which the quasicrystal pattern is transferred into the 1.5 μm SiO_2 layer. This is achieved by choosing an interlayer material that is not affected by typical etching processes used for structuring both the photoresist and the ARC layer. Here we use a 20 nm SiO_2 interlayer. Dry etching is used to "project" the photoresist structure into the 20 nm thin SiO_2 interlayer (CHF_3 RIE), and then the structure is transferred into the organic material based ARC layer using RIE with O_2 plasma. The process is shown in Figure 7d–i, with SEM images of actual samples produced in the case of line gratings (one exposure).

In **Figure 8**, we show a 2D quasiperiodic pattern with 10-fold rotational symmetry, obtained by 5 exposures. Good correspondence of the 2D decagonal quasiperiodic structure produced by IL with the mathematical Penrose tiling, comprising two rhombohedral motifs (acute angles of 36° and 72°), is evident. MEIL allows the high quality fabrication of 2D quasiperiodic structures over large areas. As an example, **Figure 9** shows the SEM image of a 40 μm × 60 μm portion of a 2D octagonal quasicrystal of a 2 cm^2 area fabricated by 4 exposures with 45° rotations.

The advantage of MEIL for fabricating 2D QCs with various rotational symmetries is presented in the **Figure 10**, where three kinds of quasicrystals were readily fabricated just by changing the number and corresponding angles of rotations. In all three cases, line gratings with 300 nm periods were recorded in each exposure. The simulation patterns predicted

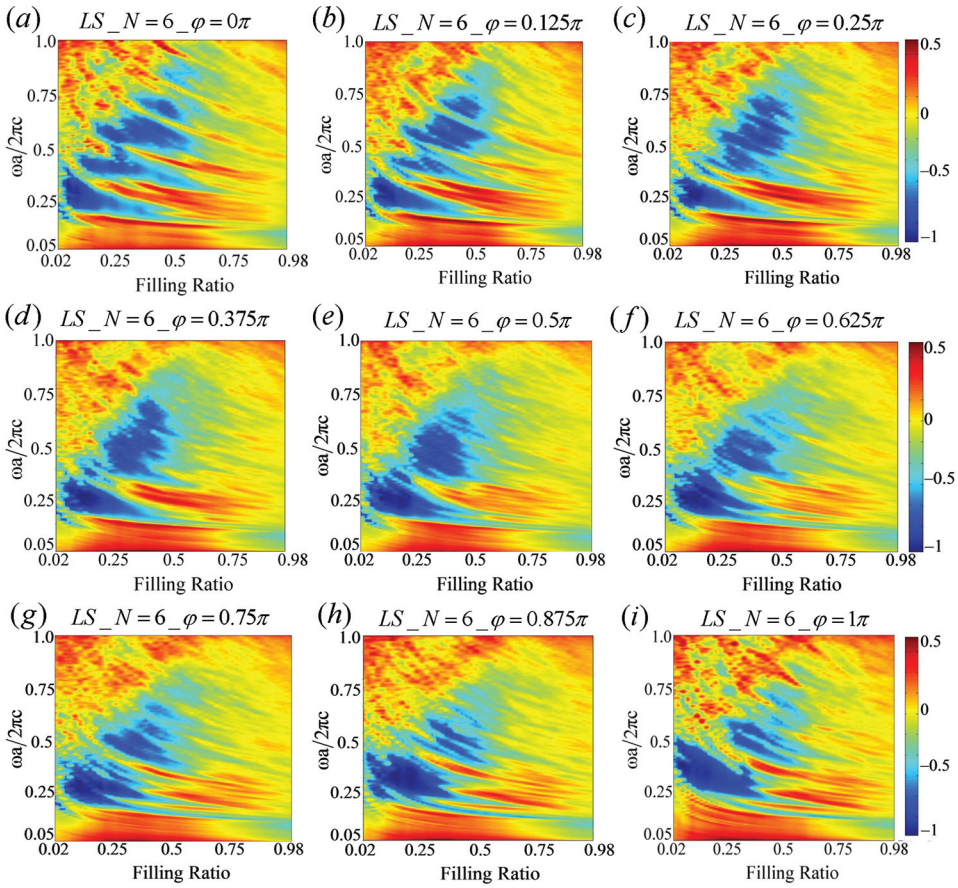

Figure 6. PBG maps for 12-fold rotational symmetric QCs.

Table 1. The largest TM PBGs according to the PBG maps. Here f is the filling ratio corresponding to the largest TM PBG.

QC type	f	ω (lower) $a/2\pi c$	ω (upper) $a/2\pi c$	ω (middle) $a/2\pi c$	$\Delta\omega/\omega$ (center)
LS _N = 4	0.18	0.22	0.32	0.27	37.0%
LS _N = 5_ $\phi = 0\ \pi$	0.24–0.38	around 0.21	around 0.28	around 0.245	around 28.5%
LS _N = 5_ $\phi = 0.125\ \pi$	0.22	0.22	0.295	0.2575	29.1%
LS _N = 5_ $\phi = 0.25\ \pi$	0.14	0.236	0.3265	0.28125	32.2%
LS _N = 5_ $\phi = 0.375\ \pi$	0.12	0.255	0.3525	0.3038	32.1%
LS _N = 5_ $\phi = 0.5\ \pi$	0.14	0.238	0.3266	0.2823	31.4%
LS _N = 5_ $\phi = 0.625\ \pi$	0.14	0.235	0.3375	0.2863	35.8%
LS _N = 5_ $\phi = 0.75\ \pi$	0.2–0.28	around 0.21	around 0.28	around 0.245	around 28.5%
LS _N = 5_ $\phi = 0.875\ \pi$	0.18	0.2175	0.32	0.26875	38%
LS _N = 5_ $\phi = \pi$	0.12	0.235	0.3425	0.289	37.2%
LS _N = 6_ $\phi = 0\ \pi$	0.14	0.225	0.34	0.2825	40.7%
LS _N = 6_ $\phi = 0.125\ \pi$	0.18	0.22	0.3225	0.271	37.8%
LS _N = 6_ $\phi = 0.25\ \pi$	0.26	0.2	0.31	0.255	43.1%
LS _N = 6_ $\phi = 0.375\ \pi$	0.22	0.21	0.315	0.2625	40%
LS _N = 6_ $\phi = 0.5\ \pi$	0.22	0.216	0.318	0.267	38.2%
LS _N = 6_ $\phi = 0.625\ \pi$	0.26	0.26	0.3075	0.284	16.7%
LS _N = 6_ $\phi = 0.75\ \pi$	0.24	0.2626	0.3284	0.2955	22.26%
LS _N = 6_ $\phi = 0.875\ \pi$	0.2	0.2725	0.4175	0.345	42%
LS _N = 6_ $\phi = \pi$	0.1–0.2	around 0.285	around 0.447	around 0.366	around 44%

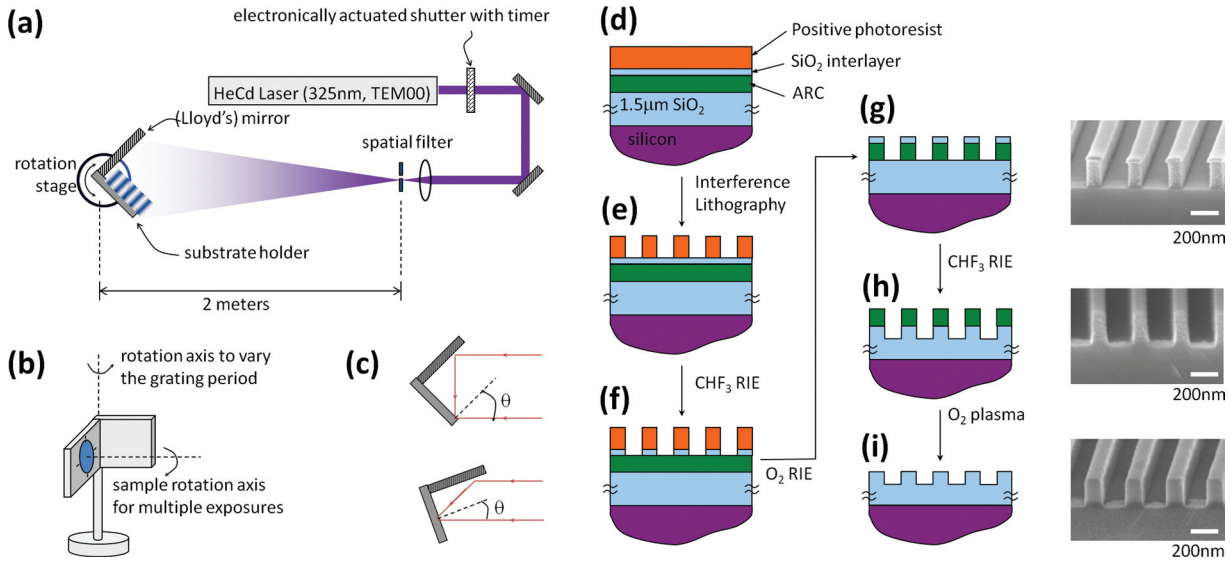

Figure 7. a) Configuration of the Lloyd's mirror interference lithography system. b) Sample holder assembly, showing the rotation axis for changing the grating periodicity, and the axis around which the substrate is rotated during MEIL. c) Rotating the entire stage assembly changes the incidence angle and thus the periodicity of the recorded gratings. d) The initial sample stack is composed of 200 nm photoresist, 20 nm SiO_2 and 200 nm organic ARC material, on a 1.5 μm thermal oxide coated silicon wafer substrate. e) The developed photoresist structure; f) the SiO_2 interlayer is etched with CHF_3 RIE using the photoresist as a mask; g) the pattern is further transferred into ARC by etching with O_2 RIE using the SiO_2 caps as a mask; h) the pattern is finally transferred to the SiO_2 substrate by CHF_3 RIE etching using the ARC as a mask; i) the final sample is obtained by stripping the ARC mask with O_2 plasma.

from Equation (2) match with the experimental results. Structural defects are seen, e.g., features which are connected and thus not fully photo-developed (Figure 10a). This is a result of development of the photoresist in regions of low contrast from the four superposed exposures. Furthermore, some thin regions in the simulation pattern (below 50 nm) are either washed off during photoresist development or suffer from incomplete photoresist development and are somewhat thicker. For example, the central circular features in Figure 10c are either broken or thicker than the simulation result shown below in Figure 10f. However, the uniformity of the structures are remarkably high, as shown in Figure 8 and Figure 9.

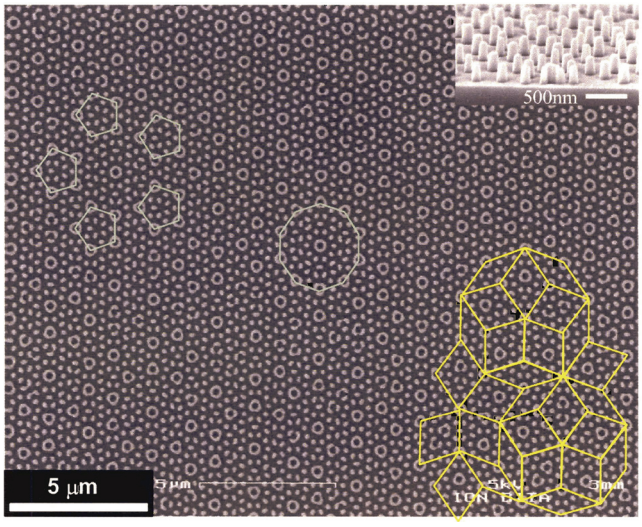

Figure 8. Plane view SEM image of a Penrose-like decagonal 2D quasiperiodic pattern etched in SiO_2. Areas with local 5 and 10 fold rotational symmetries are emphasized, and a portion of a Penrose tiling pattern is overlaid on the sample image (right side in yellow). The inset figure shows an edge-on SEM image of the same sample, where the height of the posts is 240 nm. The structure was obtained by 5 exposures with 36° rotations of the 300 nm period line gratings.

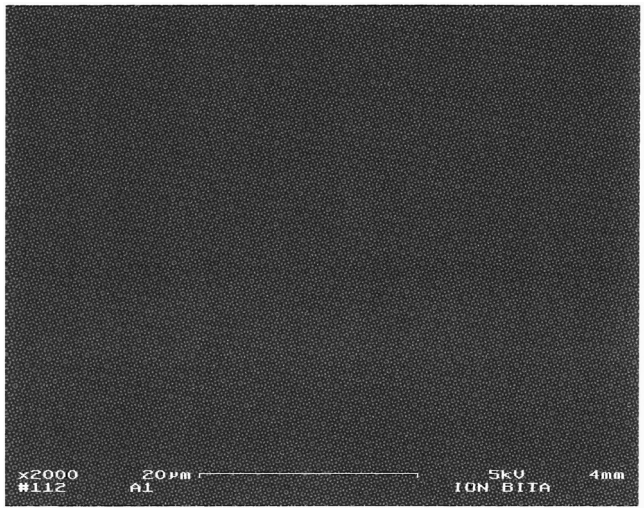

Figure 9. Large area (~40 μm × 60 μm), plan view SEM image of an octagonal 2D quasiperiodic silica structure obtained by 4 exposures of line gratings with 300 nm periodicity, and subsequent rotations with 45°.

3. Conclusions

In conclusion, the PBG properties of 8-, 10- and 12-fold QCs with nine different φ parameters and wide filling ratios (0.02–0.98) are discussed. We have found the largest TM PBGs of 8-, 10- and 12-fold QCs for different φ parameters, which are shown in Table 1. Large area and high quality 8-, 10-, and 12-fold rotational symmetric QCs with ~100 nm features made by MEIL are also demonstrated. We anticipate that this work provides guidance for future fabrication of photonic QC devices.

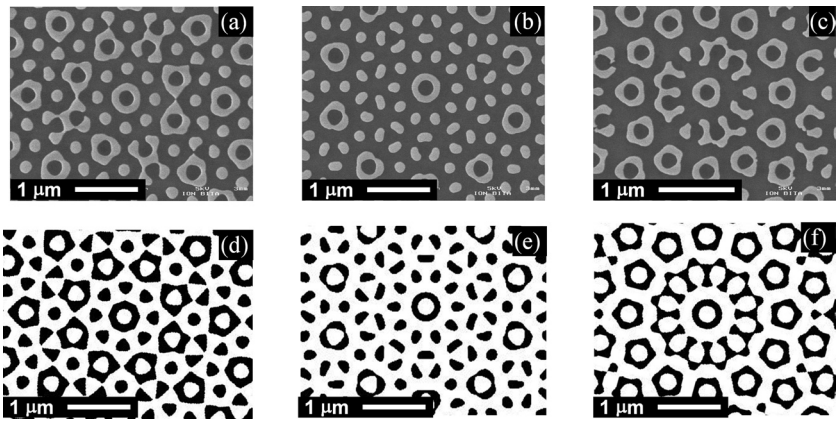

Figure 10. Plane view SEM images of 2D octagonal (a), decagonal (b), and dodecagonal (c) quasiperiodic structures produced by MEIL with N = 4, 5, and 6. Views of the central axis show 8 mm, 10 mm, and 12 mm point symmetries. (d), (e), and (f) are our simulation results from Equation (2). The theory and experiment match very well.

4. Experimental Section

The FDTD calculation of the PBG maps: a large portion of each type of QC is selected as the computation domain with perfectly matched layers at the boundaries. A set of randomly distributed radiating dipoles in the central area introduces electromagnetic waves to the computational domain and four hundred detectors are equally spaced along the perimeter. The detectors collect the transmission spectra, which represents the LDOS.

Fabrication of photonic QCs: the silicon wafer is thermal oxide-coated with a 1.5 μm SiO_2 layer. The ARC is a 220 nm thick BARLi I-line antireflection layer from AZ Electronic Materials. The 20 nm pattern transfer interlayer is deposited by e-beam evaporation and the photoresist used is the PFI-88 A3 positive photoresist from Sumitomo (Sumika) Chemical. The laser source used in MEIL is a 40 mW HeCd laser outputting TEM00 mode (325 nm wavelength). After the multiple exposures and substrate rotations, the photoresist was developed in Microsoft MF CD-26 for around 60 seconds. The quasicrystalline photoresist pattern was transferred into the SiO_2 layer via several RIE steps performed in a Plasma Therm Model 790. The detailed RIE process is shown in Figure 7.

Acknowledgements

L.J. and I.B. contributed equally to this work. This research is partially supported by the US Army Research office through the Institute for Soldier Nanotechnologies, under contract W911NF-07-D-0004; the research is also partially supported by NSF, under grant DMR-0804449.

Received: August 4, 2011
Published online: January 17, 2012

[1] C. Janot, *Quasicrystals: a primer*, Clarendon Press, New York **1994**.
[2] Y. S. Chan, C. T. Chan, Z. Y. Liu, *Phys. Rev. Lett.* **1998**, *80*, 956.
[3] M. C. Rechtsman, H. C. Jeong, P. M. Chaikin, S. Torquato, P. J. Steinhardt, *Phys. Rev. Lett.* **2008**, *101*, 073902.
[4] M. Florescu, S. Torquato, P. J. Steinhardt, *Phys. Rev. B* **2009**, *80*, 155122.
[5] K. Mnaymneh, R. C. Gauthier, *Opt. Express* **2007**, *15*, 5089.
[6] R. C. Gauthier, K. Mnaymneh, *Opt. Commun.* **2006**, *264*, 78.
[7] A. Della Villa, S. Enoch, G. Tayeb, F. Capolino, V. Pierro, V. Galdi, *Opt. Express* **2006**, *14*, 10021.
[8] S. M. Thon, W. T. M. Irvine, D. Kleckner, D. Bouwmeester, *Phys. Rev. Lett.* **2010**, *104*, 243901.
[9] L. Jia, I. Bita, E. L. Thomas, *Phys. Rev. A* **2011**, *84*, 125128.
[10] J. L. Yin, X. G. Huang, S. H. Liu, S. J. Hu, *Opt. Commun.* **2007**, *269*, 385.
[11] G. Zito, T. P. Rose, E. Di Gennaro, A. Andreone, E. Santamato, G. Abbate, *Microwave Opt. Technol. Lett.* **2009**, *51*, 2732.
[12] E. Di Gennaro, C. Miletto, S. Savo, A. Andreone, D. Morello, V. Galdi, G. Castaldi, V. Pierro, *Phys. Rev. B* **2008**, *77*, 193104.
[13] C. J. Jin, B. Y. Cheng, B. Y. Man, Z. L. Li, D. Z. Zhang, S. Z. Ban, B. Sun, *Appl. Phys. Lett.* **1999**, *75*, 1848.
[14] H. H. Tao, C. Ren, S. Feng, Y. Z. Liu, Z. Y. Li, B. Y. Cheng, D. Z. Zhang, A. Z. Jin, *J. Vacuum Sci. Technol. B* **2007**, *25*, 1609.
[15] Z. F. Yu, G. Veronis, Z. Wang, S. H. Fan, *Phys. Rev. Lett.* **2008**, *100*, 023902.
[16] M. L. Povinelli, S. H. Fan, *Appl. Phys. Lett.* **2006**, *89*, 191114.
[17] X. H. Deng, Y. G. Peng, J. T. Liu, J. R. Yuan, L. Zou, *J. Mod. Opt.* **2010**, *57*, 325.
[18] J. Ma, M. L. Povinelli, *Opt. Express* **2011**, *19*, 10102.
[19] S. Kim, C. S. Kee, *Opt. Express* **2009**, *17*, 15885.
[20] A. Gopinath, S. V. Boriskina, N. N. Feng, B. M. Reinhard, L. Dal Negro, *Nano Lett.* **2008**, *8*, 2423.
[21] K. Hwang, D. Kwak, C. Kang, D. Kim, Y. Ahn, Y. Kang, *Angew. Chem., Int. Ed.* **2011**, *50*, 6311.
[22] I. Lee, D. Kim, J. Kal, H. Baek, D. Kwak, D. Go, E. Kim, C. Kang, J. Chung, Y. Jang, S. Ji, J. Joo, Y. Kang, *Adv. Mater.* **2010**, *22*, 4973.
[23] A. Mihi, C. Zhang, P. V. Braun, *Angew. Chem., Int. Ed.* **2011**, *50*, 5711.
[24] H. Zhang, X. Yu, P. V. Braun, *Nature Nanotechnology* **2011**, *6*, 277.
[25] G. Liang, X. Zhu, Y. Xu, J. Li, S. Yang, *Adv. Mater.* **2010**, *22*, 4524.
[26] X. Zhu, G. Liang, Y. Xu, S.-C. Cheng, S. Yang, *J. Opt. Soc. Am. B-Opt. Phys.* **2010**, *27*, 2534.
[27] J. B. Yeo, S. D. Yun, N. H. Kim, H. Y. Lee, *J. Vacuum Sci. Technol. B* **2009**, *27*, 1886.
[28] I. Bita, T. Choi, M. E. Walsh, H. L. Smith, E. L. Thomas, *Adv. Mater.* **2007**, *19*, 1403.
[29] J. Xu, R. Ma, X. Wang, W. Y. Tam, *Opt. Express* **2007**, *15*, 4287.
[30] S. P. Gorkhali, J. Qi, G. P. Crawford, *J Opt. Soc. Am. B-Opt. Phys.* **2006**, *23*, 149.
[31] R. C. Gauthier, K. Mnaymneh, *Opt. Express* **2005**, *13*, 1985.
[32] L. Jia, E. L. Thomas, *Phys. Rev. A* **2011**, *84*, 033810.
[33] L. Jia, E. L. Thomas, *Phys. Rev. B* **2011**, *84*, 125128.
[34] L. Jia, E. L. Thomas, *J. Opt. Soc. Am. B-Opt. Phys.* **2009**, *26*, 1882.
[35] G. Zito, B. Piccirillo, E. Santamato, A. Marino, V. Tkachenko, G. Abbate, *J. Opt. A-Pure Appl. Opt.* **2009**, *11*, 024007.

[36] K. Busch, S. John, *Phys. Rev. E* **1998**, *58*, 3896.
[37] V. I. Kopp, B. Fan, H. K. M. Vithana, A. Z. Genack, *Opt. Lett.* **1998**, *23*, 1707.
[38] S. Y. Zhu, Y. P. Yang, H. Chen, H. Zheng, M. S. Zubairy, *Phys. Rev. Lett.* **2000**, *84*, 2136.
[39] W. S. Kim, L. Jia, E. L. Thomas, *Adv. Mater.* **2009**, *21*, 1921.
[40] R. C. Gauthier, A. Ivanov, *Opt. Express* **2004**, *12*, 990.
[41] X. Wang, C. Y. Ng, W. Y. Tam, C. T. Chan, P. Sheng, *Adv. Mater.* **2003**, *15*, 1526.
[42] G. von Freymann, W. Koch, D. C. Meisel, M. Wegener, M. Diem, A. Garcia-Martin, S. Pereira, K. Busch, J. Schilling, R. B. Wehrspohn, U. Gosele, *Appl. Phys. Lett.* **2003**, *83*, 614.